Uniaxial-planar deformation of poly(ethylene terephthalate) films: 1. Characterization of the crystalline phase

Philippe Lapersonne, Jean-François Tassin* and Lucien Monnerie
Ecole Supérieure de Physique et Chimie Industrielles de la Ville de Paris, Laboratoire de Physico-Chimie Structurale et Macromoléculaire, 10 rue Vauquelin, 75231 Paris Cedex 05, France

and Jean Beautemps
Rhône Poulenc Recherches, 85 Avenue des Frères Perret, BP 62, 69192 Saint Fons, France
(Received 6 August 1990; revised 15 October 1990; accepted 18 October 1990)

Amorphous isotropic poly(ethylene terephthalate) films were deformed under uniaxial-planar symmetry conditions at constant engineering stress close to and above the glass transition temperature. The structure of the crystalline phase is characterized in terms of orientation, size and organization of the crystalline blocks by X-ray scattering techniques. The orientation of the crystallographic axes and the size of the crystalline blocks are well rescaled by the macroscopic draw ratio, which is a function of the drawing temperature and the applied stress. The large-scale organization of the crystalline phase is not determined by the same parameter but changes mainly with temperature.

(Keywords: deformation; poly(ethylene terephthalate); film; characterization; X-ray scattering; biaxial deformation orientation)

INTRODUCTION

One of the most important preparations of poly(ethylene terephthalate) (PET) is flat film processing. In one of the processes, the first step is drawing between rollers followed by transverse stretching in an oven. The structure of the film after the first deformation process is of great importance for the second one, justifying an accurate study of this longitudinal stretching. Owing to the constraint imposed on the film during the first drawing stage, the deformation possesses a uniaxial-planar symmetry instead of an axial one. The drawing scheme is characterized by a constant drawing force[1].

A stretching machine designed to deform the samples under constant load has been set up recently, and the kinematics of the deformation as well as the initial measurements on the structure of the deformed samples have been reported[2,3].

In this series of papers we wish to describe the structure of the deformed films obtained using this type of deformation under different conditions of load and temperature. This paper is devoted to the characterization of the crystalline phase, emphasizing the aspects of crystallinity, orientation and organization of the crystalline phase. Most of the information has been extracted from X-ray scattering experiments at wide as well as at small angles. Although many studies on the orientation of deformed PET films, based on X-ray measurements, either at wide[4–14] or at small angles[14–19], have been reported for uniaxial or biaxial types of orientation, the detailed influences of the stretching conditions on the structure of the film cannot be drawn out easily. However, our work follows much of these earlier reports since the same means of investigations have been used here. In addition to the quantitative structural characterization of the films, emphasis will be given to the precise influence of the macroscopic parameters (draw ratio, temperature, stretching time) on the morphology of the samples.

EXPERIMENTAL

Sample preparation

Amorphous isotropic PET films (thickness 160 μm) were supplied by Rhône Poulenc Recherches. In order to allow polarized fluorescence measurements, these films were labelled at a concentration of 100 ppm (by weight) with a photostable compound 4,4'-(dibenzoxazolyl)-stilbene (VPBO) introduced during the polycondensation reaction. Fluorescence polarization data will be reported in part 2 of this series. The weight-average molecular weight was 39 000 as determined by viscosimetry in *o*-chlorophenol at 25°C. The glass transition temperature T_g as measured by d.s.c. at a heating rate of 20°C min^{-1} was 80°C.

Rectangular samples were cut and fitted to the grips of the stretching machine so that the initial deformable size was 10 mm long and 120 mm wide. In order to deform the sample, a given load was hung on the lower grip, the upper one being fixed. The sample is thus deformed under a constant engineering stress. Different

* To whom correspondence should be addressed at: Université du Maine, Faculté des Sciences, Avenue Olivier Messiaen, 72017 Le Mans, France

0032-3861/91/183331-09

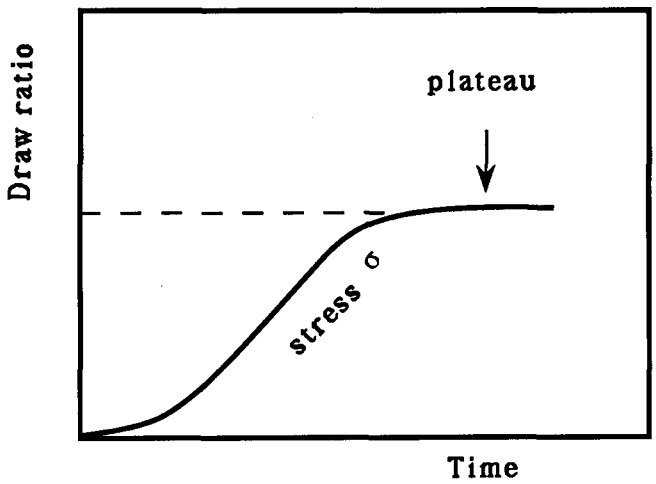

Figure 1 Schematic variation of the deformation under constant load as a function of time

samples were produced by varying the conditions of load and temperature. The kinematics of this stretching process has been accurately described in ref. 2. We briefly recall that in such an experiment the deformation varies with time as shown in *Figure 1*. In the first regime, the deformation increases rapidly with time (typical timescales are of course a function of load and temperature and can be found in ref. 2). It then levels off and reaches an equilibrium plateau value also dependent on load and temperature. If the state of orientation inside the sample is quenched just after (say within 1 or 2 s) the deformation has reached its equilibrium value, the stretching is defined as 'drawing with a short plateau'. The orientational states existing before the equilibrium situation can also be frozen in by setting the required deformation to a value less than the equilibrium value and quenching the sample just as it reaches the chosen deformation. Such stretching is referred to as 'drawing with quenching' and will not be considered here.

In this paper, only samples 'drawn with a short plateau' will be studied. They were obtained by varying the temperature in the range 85–110°C and the engineering stress between 1.23 and 5.52 MPa. The different measurements were carried out on the central portion ($8 \times 2\ cm^2$) of the samples where the deformation is characterized by a constant width, and thus it has a uniaxial-planar symmetry, as checked by ink grids.

Sample characterization

Refractive index measurements. An Abbe refractometer under polarized light has been used to measure the refractive indices in the three principal directions. Only the average index of refraction will be considered here and used to characterize the density of the film using the following expression derived for PET films[20]:

$$d = 4.047\left(\frac{\bar{n}^2 - 1}{\bar{n}^2 + 2}\right) \qquad (1)$$

This relation is independent of the degree of crystallinity and the level of orientation.

Crystallinity. The degree of crystallinity was determined by assuming a non-interpenetrated two-phase model, with a density of the crystalline phase $d_c = 1.455\ g\ cm^{-3}$ and of the amorphous phase $d_a = 1.335\ g\ cm^{-3}$:

$$\chi = \frac{d - d_a}{d_c - d_a} \qquad (2)$$

Such a relation implies that any densification in the sample is attributed to an increase in crystallinity. According to Nobbs *et al.*[8], up to a level of orientation of the amorphous phase equal to 0.4 the density of the amorphous phase does not exceed $1.342\ g\ cm^{-3}$. Such a variation has negligible consequences for moderate crystallinities (0.2 or higher) but its effect makes the onset of crystallinity difficult to distinguish from a densification of the amorphous phase.

Wide-angle X-ray scattering. The wide-angle X-ray scattering experiments were conducted on a Philips PW1050 diffractometer equipped with a rotation device. The intensities were corrected for background scattering.

The samples were prepared by stacking 1 cm square pieces of the oriented film so as to obtain a thicker film yielding sufficient intensity. The unit cell was taken from the work of de Daubeny, Bunn and Brown[21]. It has triclinic symmetry with $a = 4.56$ Å, $b = 5.94$ Å, $c = 10.75$ Å and $\alpha = 98.5°, \beta = 118°, \gamma = 112°$. The c axis lies along the chain direction and the plane of the phenyl rings is roughly perpendicular to the a axis. Attention was given to the (0 1 0), (1 0 0) and ($\bar{1}$ 0 5) crystallographic planes. Although the normal to the (1 0 0) plane is slightly inclined ($\approx 19°$) with respect to the normal to the phenyl ring, information concerning the orientation of the plane of the phenyl ring can be obtained from this reflection. The diffraction from the ($\bar{1}$ 0 5) plane is usually studied to yield information about the orientation of the chain axis, but here also a slight angle exists between the c axis and the ($\bar{1}$ 0 5) plane normal.

Determination of the size of the crystallites. The size of the crystallites in the direction normal to the ($\bar{1}$ 0 5), (1 0 0) and (0 1 0) planes has been determined from the angular broadening of the diffraction peaks using the Scherrer formula[22]:

$$L_{hkl} = \frac{\lambda}{\Delta\theta_{hkl} \cos\theta_{hkl}} \qquad (3)$$

in which $\Delta\theta_{hkl}$ is the angular width at half height at the Bragg angle θ_{hkl} corrected for the experimental width at this angle. The intensities around the θ_{hkl} direction were recorded using a one-dimensional position-sensitive detector coupled with a multichannel analyser and the sample was positioned in the X-ray beam so as to maximize the diffracted intensity.

Determination of the orientation. We now wish to characterize quantitatively the crystalline orientation inside the sample. This is equivalent to defining the average position of the crystallographic unit cell (i.e. a, b or c crystallographic axes or various crystallographic plane normals) with respect to the principal directions of the sample (i.e. the machine, transverse and normal directions).

Mathematical characterization of the orientation. Let us consider a system of axes $OX_1X_2X_3$ attached to the

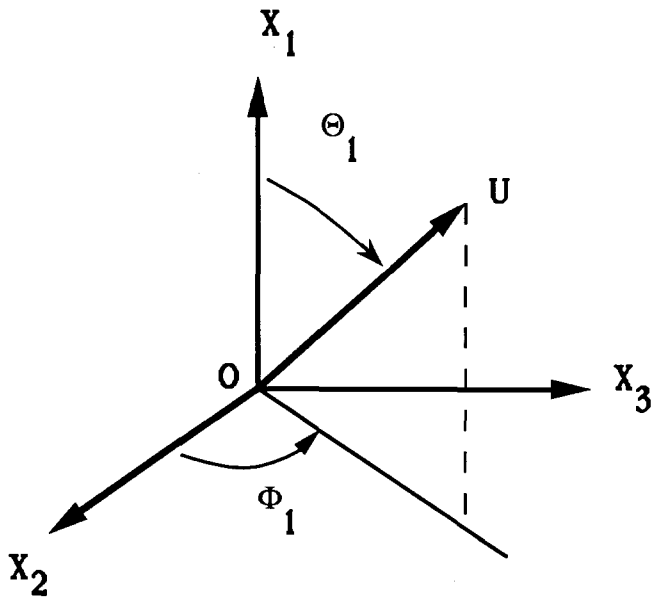

Figure 2 Definition of the angular coordinates (Θ_1 and Φ_1) of a vector U with respect to the system of axes $OX_1X_2X_3$. Throughout this paper OX_1 is taken as the draw or machine direction, OX_2 as the transverse direction and OX_3 is parallel to the film normal

sample. The subscripts 1 and 2 refer to the principal axes in the plane of the film (1 being the machine and 2 the transverse direction) and the OX_3 axis is perpendicular to this plane. Our purpose is to describe the orientation of a unit vector U. A reference axis OX_i with $i = 1, 2$ or 3 can be chosen and the orientation of U with respect to OX_i can be specified by the angles Θ_i and Φ_i as illustrated in *Figure 2*. (In this paper the angles of the vectors with respect to the reference axes will be designated by capital Greek letters, whereas lower-case letters will be used for experimental angles, like the Bragg angle.)

This orientation can be described by an orientation distribution function $N^{u,i}(\Theta_i, \Phi_i)$ from which different momenta (averages of generalized Legendre polynomials) can be derived. Hereafter, $P^{u,i}_{200}$ and $P^{u,i}_{220}$ will be considered. These quantities have the following expressions as functions of the angles Θ_i and Φ_i:

$$P^{u,i}_{200} = \tfrac{1}{2}\langle 3\cos^2\Theta_i - 1\rangle \quad (4)$$

$$P^{u,i}_{220} = \tfrac{1}{4}\langle (1-\cos^2\Theta_i)\cos 2\Phi_i\rangle \quad (5)$$

(Note that $P^{u,i}_{220} = \frac{1}{6}(P^{u,j}_{200} - P^{u,k}_{200})$ where indices j and k refer to the two other directions so that X_i, X_j and X_k make a direct system of axes.) Orientation measurements are often performed from pole figures. Unfortunately, our X-ray equipment does not allow us to produce pole figures so that a somewhat different procedure has been used. The angles considered in the X-ray diffraction set-up are shown in *Figure 3* where the sample is positioned for a transmission experiment.

Orientation of the chain axes. The ($\bar{1}$ 0 5) planes diffract the X-rays around a Bragg angle $2\theta = 42.6°$. To measure the distribution of the chain axes in the plane of the film, the detector was set at the angle maximizing the diffracted intensity. The sample was then rotated 2π around the 3 axis (angle φ varies from 0 to 2π) yielding an azimuthal sweep. The recorded intensity reflects the distribution of the ($\bar{1}$ 0 5) planes normal (i.e. roughly the chain axes) in the plane of the film $N^{\bar{1}05,1}(\Theta_1, 0)$. To obtain the orientation in the 3–1 plane (i.e. perpendicular to the plane of the film), for an azimuthal angle $\varphi = 0$, the angle ψ was varied between -20 and 20°, which is the maximum range available with this equipment. The intensities were corrected for the differences in the X-ray path inside the sample as the angle ψ varies. This last angular scan reflects the distribution $N^{\bar{1}05,1}(\Theta_1, 90)$ for $-20 < \Theta_1 < 20$. In both cases, a single maximum in the intensity was observed at $\varphi = 0$ or $\psi = 0$. The second moments of the distribution of the ($\bar{1}$ 0 5) plane normals with respect to the directions 1, 2 and 3 have been evaluated assuming an elliptical distribution in the 2–3 plane, the principal axes of which are coincident with axes 2 and 3. A program has been written to compute $\langle\cos^2\Theta\rangle$ with respect to the axes 1,2,3 from the widths at half height of the distribution in the 1–2 and 1–3 planes that were fitted by a Gaussian function. This method allows the determination of $P^{\bar{1}05,1}_{200}$ and $P^{\bar{1}05,1}_{220}$.

Orientation of the planes of the phenyl rings. As the phenyl rings are known to orient preferentially in the plane of the film, a reflection set-up was preferred for studying the orientation of the (1 0 0) planes. Their orientation was determined with respect to the 3 axis. The detector was fixed at an angle $2\theta = 26°$ and the sample was rotated around the OX_1 axis yielding the distribution $N^{100,3}(\Theta_3, 90)$ and around the OX_2 axis yielding the distribution $N^{100,3}(\Theta_3, 0)$. In these two cases, only a limited range of angles was swept ($-60 < \omega$, $\varphi < 60°$). The same method as above was used to calculate $P^{100,3}_{200}$ and $P^{100,3}_{220}$.

Small-angle X-ray scattering. Small-angle X-ray scattering experiments were performed with a 12 kW Rigaku Denki rotating-anode equipment using a standard photographic method (Kiesig camera with pinhole collimation, sample–film distance 400 mm). The samples were prepared by cutting 1 mm wide strips from the deformed films and stacking them together. The X-ray beam was in the 1–2 plane, parallel to the OX_2 axis. Typical exposure times were on the order of 4 h. The diagrams were quantitatively interpreted using a microdensitometer.

RESULTS

Draw ratio

As a load is attached to the sample, and the sample is free to deform at a given temperature T above T_g, an

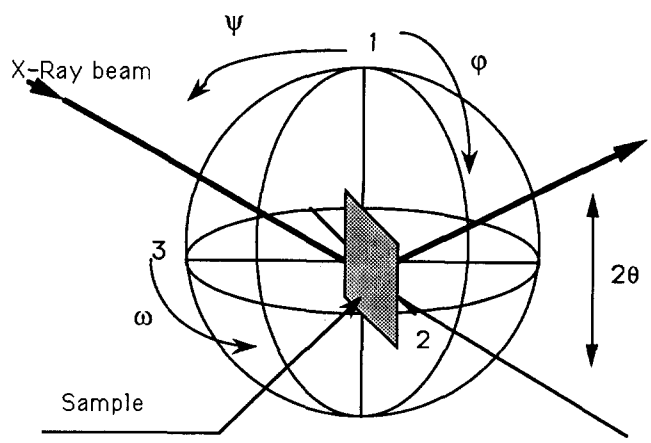

Figure 3 Position of the film in the X-ray diffractometer in a transmission experiment and definition of the experimental angles

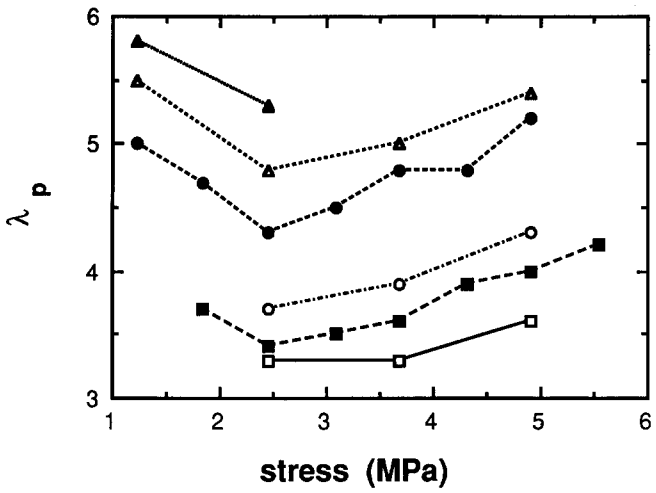

Figure 4 Plateau draw ratio λ_p *versus* applied stress for various stretching temperatures: □, 85°C; ■, 90°C; ○, 95°C; ●, 100°C; △, 105°C; ▲, 110°C. The lines are guides for the eye

equilibrium plateau deformation $\lambda_p(\sigma_0, T)$ is reached after a short time. The variation of $\lambda_p(\sigma_0, T)$ with σ_0 and T is given in *Figure 4*. For a given load, i.e. a given applied stress, the plateau deformation ratio decreases as the temperature decreases, and at fixed temperature, the plateau deformation goes through a minimum, which will be called the natural draw ratio (*NDR*).For stresses lower than the one associated with the *NDR*, the equilibrium deformation increases with decreasing stress, and this behaviour has been attributed to the combination of chain slipping and stretching rate, since small loads induce a slow stretching and therefore an easy flow of the chains. These stretching conditions are called 'stretching with flow'. For stresses above the *NDR*, the deformation at equilibrium increases with the applied stress. This means that in spite of the crystallization occurring during stretching and leading to an increase in modulus, the applied stress allows a further deformation, which is larger and larger as the applied tension is increased. This behaviour is referred to as 'crystallizing stretching'. It is worth noting that, at a given temperature, the same equilibrium deformation can be reached with two completely different types of stretching, making this distinction necessary.

Crystallinity

For the stretchings with a short plateau depicted in *Figure 4*, the density has been measured, and the crystallinity as a function of load and temperature for the same samples is plotted in *Figure 5*. As expected, the crystallinity increases with temperature and applied stress. However, the amount of crystallinity seems more sensitive to the temperature than to the stress.

In order to investigate this further, we have plotted the crystallinity *versus* plateau deformation, λ_p, in *Figure 6*. The data corresponding to the stretching with flow have been rejected from this analysis. The crystallinity developed under the crystallizing stretching conditions appears to be correlated with the equilibrium deformation. This quantity, which characterizes in a way the stretching under constant tension, is a valuable correlation parameter for the crystallinity. This rescaling with λ_p is not trivial, since the same value of λ_p can be obtained with different stresses and temperatures. It may be correlated with the fact that an equilibrium deformation is reached owing to the balance of the applied stress and the increase of the modulus of the sample due to orientation and the appearance of crystallinity.

It now seems appropriate to check whether this parameter also controls microscopic parameters like the crystalline orientation.

Crystalline orientation

Orientation of the chain axes c ((1̄ 0 5) *plane normals*) *with respect to the draw direction.* In *Figure 7* is plotted the second moment of the distribution of the (1̄ 0 5) plane normals with respect to the direction 1, $P_{200}^{\bar{1}05,1}$, *versus* λ_p for the samples stretched under crystallizing stretching conditions, whatever the applied stress or temperature. Here, also, this parameter affords a good correlation for the orientation of the crystallites. High values of orientations are observed as expected for a crystallization under tension. On the same figure, we have reported the predicted value of the orientation using the Gaylord model in uniaxial planar symmetry. The order of magnitude of the orientation is well predicted but the

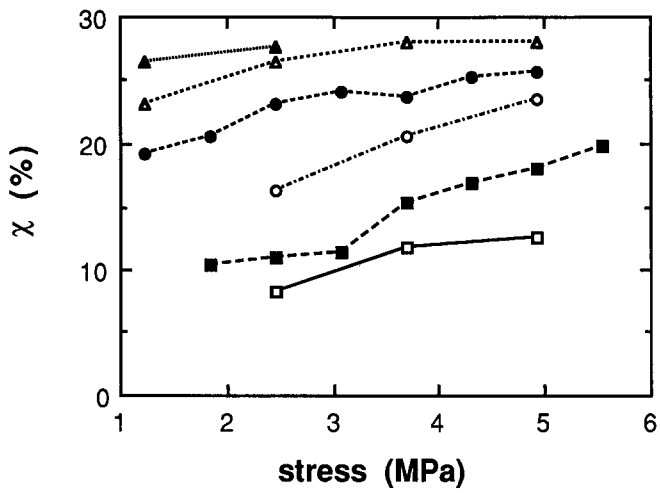

Figure 5 Crystallinity *versus* applied stress for stretching temperatures of 85, 90, 95, 100, 105 and 110°C. Same symbols as in *Figure 4*

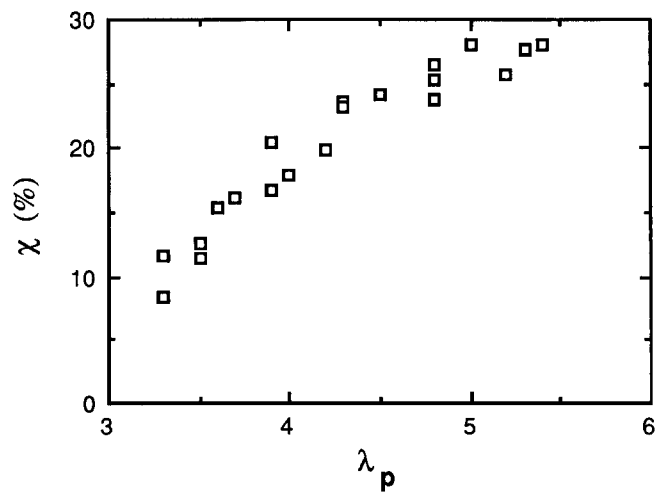

Figure 6 Crystallinity of samples stretched under 'crystallizing stretching' conditions *versus* the plateau draw ratio

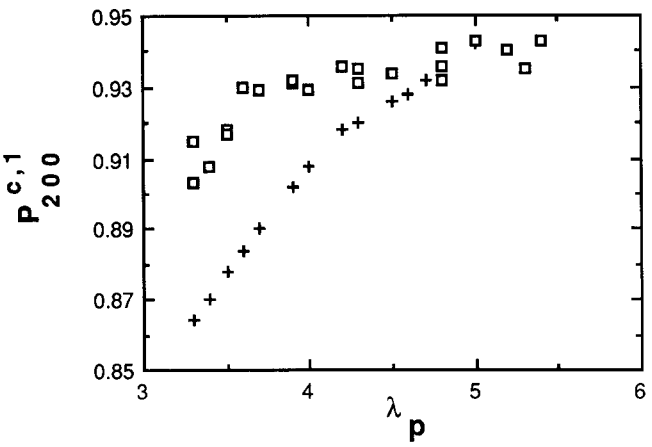

Figure 7 Orientation of the ($\bar{1}$ 0 5) plane normals with respect to the draw direction ($P^{105,1}_{200}$) *versus* the plateau draw ratio (□). Crosses refer to the predictions of the Gaylord model

experimental values are higher than anticipated especially at the lowest deformations.

As a very high orientation of the ($\bar{1}$ 0 5) plane normals in the direction of stretch is observed, they are almost perpendicular to the directions 2 and 3, so that the $P^{\bar{1}05,1}_{220}$ values are very low (of the order of 0.001 to 0.003). Because of this very small value, no typical evolution of $P^{c,1}_{220}$ with λ_p can be discerned. However, this small positive value indicates that more chain axes tend to lie in the plane of the film (1–2) than perpendicularly (1–3 plane). The difference is however quite small.

Orientation of the phenyl rings ((1 0 0) planes) with respect to the thickness direction (3). The $P^{100,3}_{200}$ data for the same set of samples are reported in *Figure 8a*. The planes of the phenyl rings tend to align parallel to the plane of the film as the deformation at equilibrium increases. The levels of orientation are much lower than those of the chain axes. Here again, λ_p is an appropriate correlation parameter.

The $P^{100,3}_{220}$ values can be used to calculate the orientation of the 1 0 0 direction with respect to the 1 and 2 axes, namely $P^{100,1}_{200}$ and $P^{100,2}_{200}$. A relatively constant value of -0.48 is obtained for $P^{100,1}_{200}$, indicating that the normal to the phenyl rings remains essentially perpendicular to the draw direction, whatever the draw ratio. As λ_p increases, a decrease of $P^{100,2}_{200}$ is observed as illustrated in *Figure 8b*. It reveals that the phenyl ring normals tend to become more and more perpendicular to the transverse direction as the deformation increases. In other words, the crystalline blocks tend to rotate around the machine direction so as to align the phenyl rings in the plane of the film.

Morphology of the crystalline phase

Crystal size. The size of the crystallites along the three principal directions of the unit cell has been measured for all the samples. The evolutions of the crystal dimensions with the applied stress at different temperatures are given in *Figures 9a, 9b* and *9c* for the crystalline directions 1 0 0, 0 1 0 and $\bar{1}$ 0 5 respectively. Hereafter, for the sake of simplicity, we will assume that the dimensions of the crystalline blocks along the principal directions *a*, *b* and *c*, denoted L_a, L_b and L_c, are equal to L_{100}, L_{010} and $L_{\bar{1}05}$ respectively.

Figure 9a shows that, at a given temperature, the size of the crystallites along the 1 0 0 direction (L_{100}) is independent of the applied stress. It is therefore a fingerprint of the stretching temperature. The growth of the crystals along this direction seems therefore to be preferentially controlled by the thermodynamics rather than by the kinetics.

The behaviour along the 0 1 0 direction is given in *Figure 9b*. A smooth increase in the size of the crystals along this direction (L_{010}) is observed as the applied stress is increased. In this case, temperature and to a lesser extent stress are acting on the crystallization. By comparing *Figures 9a* and *9b*, it can be seen that, at a given stress, an increase in temperature has roughly the same effect on the size of the crystals along these two directions. This indicates a rather similar activation energy of crystallization.

As far as the $\bar{1}$ 0 5 direction is concerned (*Figure 9c*), the size ($L_{\bar{1}05}$) of the crystals increases with the applied stress and levels off at the highest stresses. A slightly lower activation energy is found for the crystallization along this direction. However, the kinetics of crystallization is slower, so that it becomes sensitive to the applied stress and not only to temperature.

The evolution of crystallite size along the directions 1 0 0, 0 1 0 and $\bar{1}$ 0 5 is plotted in *Figure 10 versus* the plateau draw ratio for crystallizing stretchings. This parameter affords a convenient correlation for the crystal sizes along the three directions. It has to be pointed out that, for a given λ_p, the crystallites are made of roughly

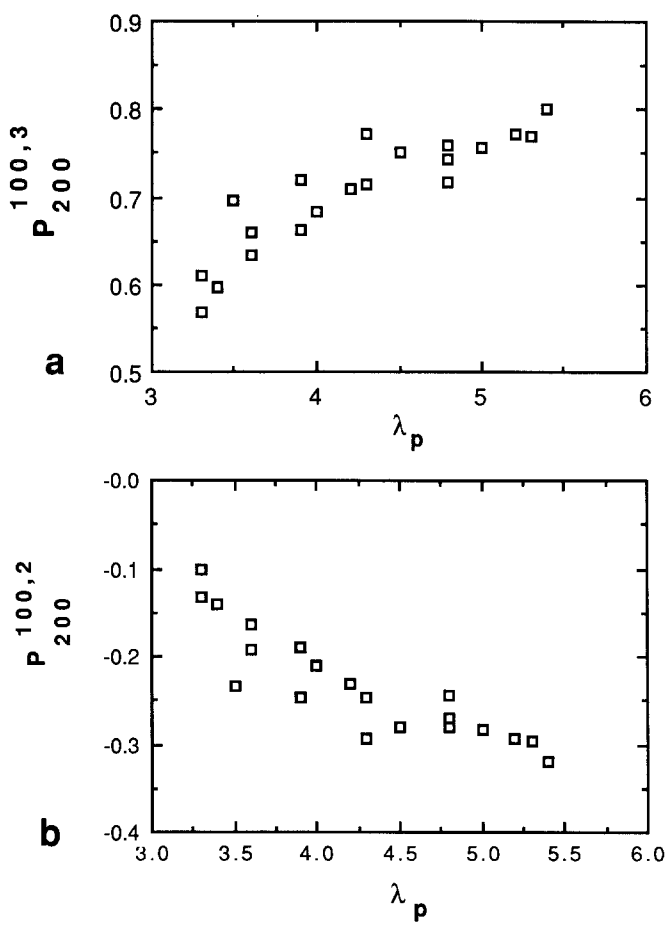

Figure 8 Orientation of the (1 0 0) plane normals with respect to (a) the thickness direction ($P^{100,3}_{200}$) and (b) the width direction ($P^{100,2}_{200}$) *versus* the plateau draw ratio

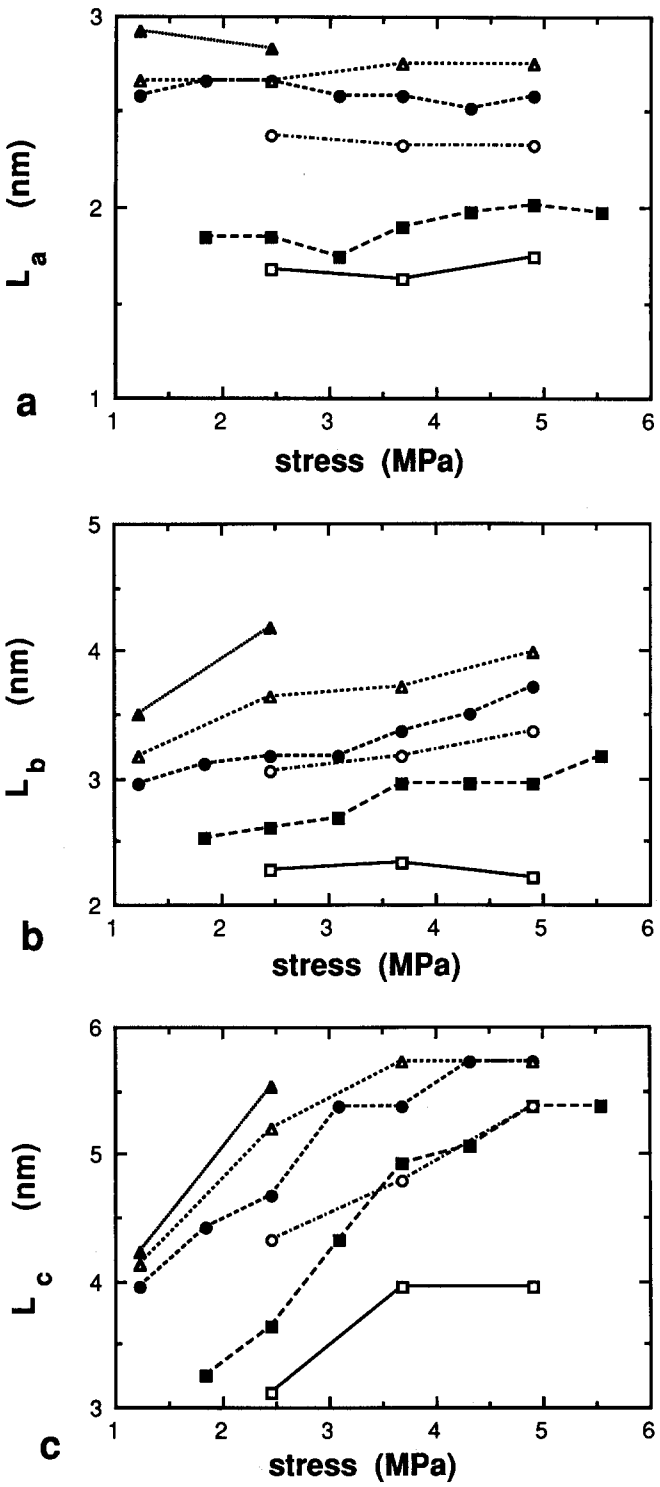

Figure 9 Crystal sizes along directions *a*, *b* and *c versus* the applied stress at different temperatures are shown in parts (a), (b) and (c) respectively. Same symbols as in *Figure 4*

the same number of unit cells stacked along the directions *a*, *b* and *c*. As an example, for $\lambda_p = 5$, the size of the crystallites along directions *a*, *b* and *c* corresponds to 7.3, 6.5 and 5.3 unit cells respectively.

Number of crystals. The number of crystals per unit volume has been evaluated as $\chi/L_{100}L_{010}L_{\bar{1}05}$. Its evolution with applied stress for the various temperatures is given in *Figure 11* under crystallizing stretching conditions. An increase in temperature induces larger crystals, so that the number of crystals per unit volume decreases. This behaviour is particularly enhanced between 85 and 90°C. The influence of the applied load is more complex. At 85°C, the number of crystals still increases as the stress is increased. The nucleation process seems therefore to be sensitive to the applied load at this temperature. At intermediate temperatures (90–95°C), the stress has no significant influence, which means that the nucleation process is completed at the lowest loads. At higher temperatures, the number of crystals decreases with the applied stress, which may reveal the coalescence of some crystalline blocks under these conditions.

Crystal organization

SAXS diagrams and direct consequences. Small-angle X-ray scattering experiments performed on all the samples show four-point patterns (under the conditions described above). The analysis of this type of pattern has been carried out by Jungnickel[23]. According to these authors, the crystallites are gathered in the film thickness direction along layers inclined at an angle α with the stretching direction, which can be determined from the SAXS diagram. Two different types of four-point patterns have been considered. They are sketched in *Figure 12* together with the proposed structure. The type A pattern corresponds to an arrangement of crystalline blocks with

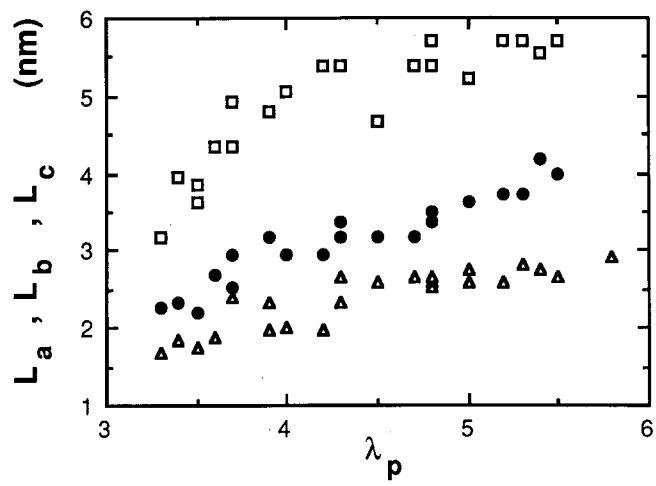

Figure 10 Crystal size along directions *a* (△), *b* (●) and *c* (□) *versus* the plateau draw ratio

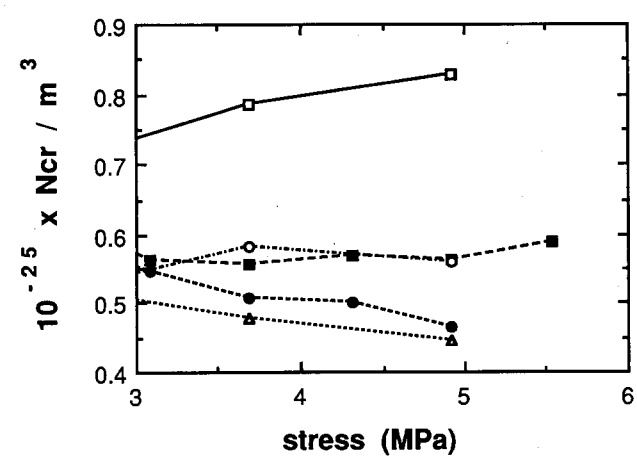

Figure 11 Number of crystals per unit volume *versus* the applied stress, under 'crystallizing stretchings', at different temperatures. Same symbols as in *Figure 4*

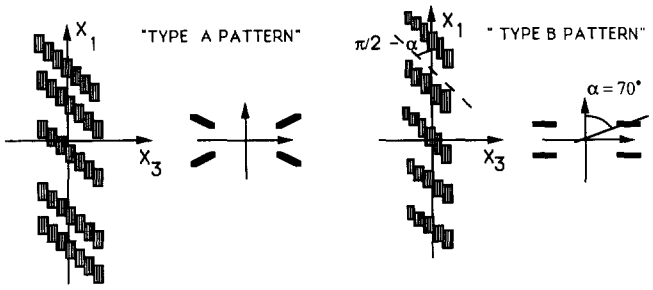

Figure 12 Schematic drawing of the SAXS diagrams and the corresponding proposed structure (after ref. 23)

a rather narrow distribution of sizes aligned along inclined layers. The interlayer distance presents large fluctuations around its average value. Type B pattern is attributed on the contrary to regularly spaced layers but bearing crystallites with a large distribution of sizes.

Samples stretched under crystallizing stretching conditions above the *NDR* exhibit SAXS patterns of the B type except for those stretched at 85°C. In this case, a very poor contrast is observed and the patterns appear intermediate between A and B type. Intermediate diagrams are also observed for the samples stretched at the *NDR* and under 'stretching with flow' conditions.

For all the samples, whatever the type of stretching, temperature or stress, the angle of inclination of the crystalline layers with the OX_1 direction is constant and has the value $70° \pm 3°$. A constant value of the inclination of the crystalline layers has also been reported by Cakmak *et al.*[14]. According to these authors, this fixed value has been encountered for different deformation tensors and has been ascribed to the crystal structure of PET. In our case, the layers are much more inclined with respect to the drawing direction. We believe that the origin of this difference relies on the processing conditions. In our case, the films are stretched very rapidly (the typical timescale is of the order of seconds) whereas a stretching rate of 800% min^{-1} has been used in the other experiments. Therefore, the crystalline organization does not seem to be based only on the crystal structure but also on the processing conditions.

The long spacing L has been evaluated for all the samples and is plotted against the applied stress at different temperatures in *Figure 13*. Except for 85°C, a limiting value ($L = 16$ nm) is observed, which is independent of the applied stress or the temperature. The higher the temperature, the smaller the stress required to reach the equilibrium value. With our data, it is difficult to state whether, at 85°C, the limiting value of L is higher or would be the same if higher stresses were used.

When the crystalline structure becomes well organized (i.e. for crystallizing stretchings above the *NDR* and for temperatures of 90°C and above), more information can be extracted from these experiments. Indeed, the results of the SAXS experiments can be combined with our data on the crystallinity and on the size of the crystals to improve our knowledge of the crystalline organization.

Evolution of the crystalline organization with stress and temperature. The thickness of the amorphous phase between crystalline layers can be calculated as $L - L_{\bar{1}05}$, where $L_{\bar{1}05}$ is the length of the crystals along the direction $\bar{1}$ 0 5 (i.e. roughly along the OX_1 direction). It is reported as a function of the applied stress for the different temperatures in *Figure 14*. The thickness of the interlayer amorphous phase rapidly reaches a constant value independent of the applied stress and the temperature. Although a slight increase of $L_{\bar{1}05}$ with temperature has been observed, it does not significantly alter the thickness of the amorphous phase since the long period, which is measured within an uncertainty of ± 1 nm, is much larger than $L_{\bar{1}05}$. Therefore, even if the equilibrium draw ratio is changed, owing to temperature or stress effects, the crystalline organization inside the material can be considered as unchanged within our experimental error.

Nevertheless, an increase in crystallinity with the applied stress or the temperature has been noted. Taking into account the fact that the overall morphology is unchanged, this increase in crystallinity can only be explained by a thickening of the crystalline layers along the three principal directions. This rules out any nucleation and growth process outside the crystalline layers, whatever the temperature and the applied stress. It is worth noting that an increase of the crystal size along directions 1 0 0 or 0 1 0 leads to an increase of the crystalline volume fraction inside a layer.

Our purpose is now to discuss how this may occur and what are the effects of the macroscopic parameters.

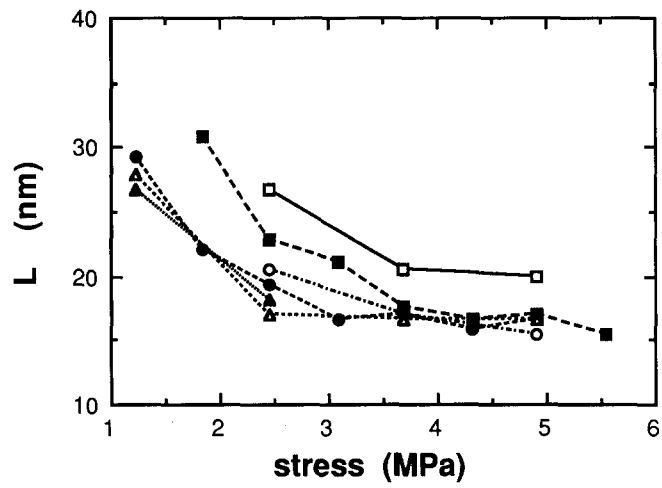

Figure 13 Long spacing *versus* the applied stress at different temperatures. Same symbols as in *Figure 4*

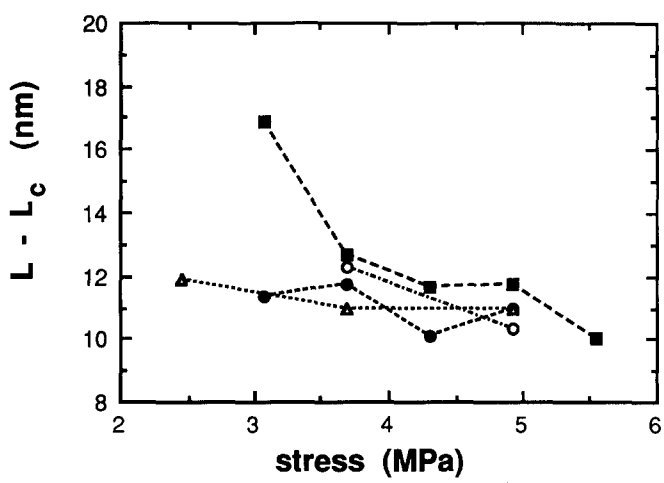

Figure 14 Thickness of the amorphous phase *versus* the applied stress at different temperatures above 90°C. Same symbols as in *Figure 4*

The crystalline volume fraction inside a layer can be evaluated as follows. If all the crystallites within a layer are touching their neighbours, then the maximum crystallinity is reached and it can be expressed as the number of crystalline layers per unit length ($1/L$) times the thickness of a crystalline layer (L_c), so that:

$$\chi_{max} = L_c/L \quad (6)$$

On the other hand, if inhomogeneities are present inside a layer, a lower overall crystallinity χ is observed, which can be used to evaluate the mean crystallinity inside a layer as:

$$\bar{\chi} = \chi/\chi_{max} = \chi L/L_c \quad (7)$$

This quantity can also be written as proportional to the number of crystalline blocks per layer (N_l) times their sizes along the directions 1 and 2, so that:

$$\bar{\chi} \propto N_l L_a L_b \quad (8)$$

In *Figure 15*, the mean crystallinity inside a layer has been plotted *versus* the applied stress for different temperatures. Under crystallizing stretching conditions, at a given temperature, it is almost independent of the applied stress and decreases as the temperature is lowered. Since the long period is constant, independent of either stress or temperature, the increase of the bulk crystallinity with the applied stress arises mainly from a thickening of the crystalline blocks along direction c. This conclusion is in agreement with the respective influences of stress and temperature on the crystallite size along directions a, b and c. At a given temperature, both the mean crystallinity $\bar{\chi}$ and the crystal length along direction a are independent of the stress so that, from equation (8), it follows that $N_l L_b$ is also independent of the stress. This is successfully checked in *Figure 16*. It can also be remarked that $N_l L_b$ is also independent of temperature.

The evolution of N_l with the temperature and the applied stress is given in *Figure 17*. A decrease of the number of crystalline blocks per layer is observed when either temperature or load is increased. The influence of temperature is dominant, however. Since an increase in L_b with the applied load has already been observed (see *Figure 9b*), the decrease of the number of crystal blocks per layer can be attributed to either the existence of larger

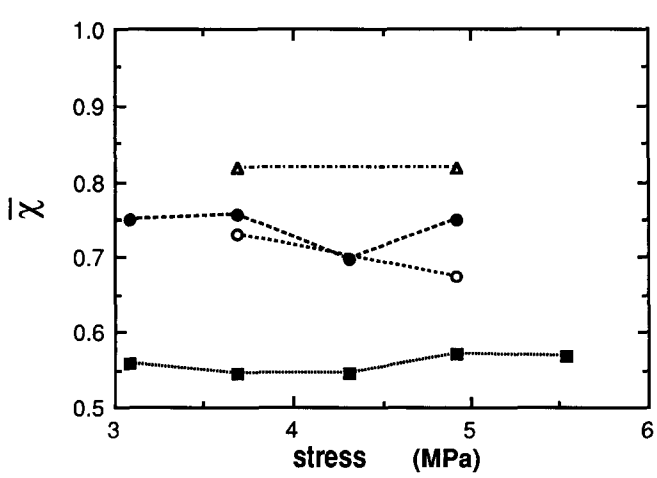

Figure 15 Mean crystallinity inside a crystalline layer *versus* the applied stress at different temperatures above 90°C. Same symbols as in *Figure 4*

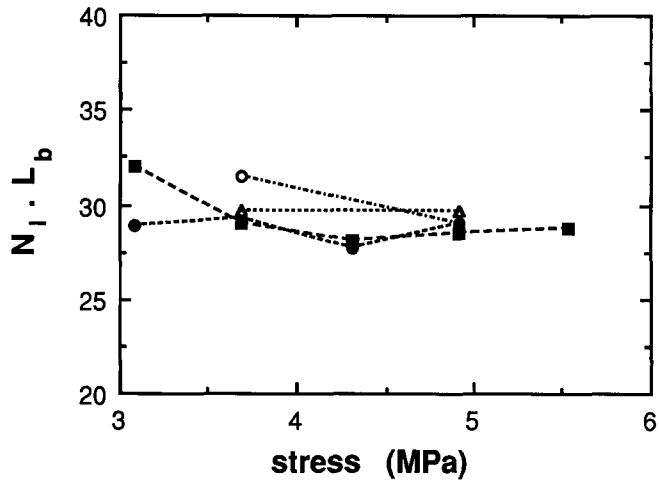

Figure 16 Evolution of the quantity $N_l L_b$ (see text) *versus* the plateau draw ratio for different temperatures. Same symbols as in *Figure 4*

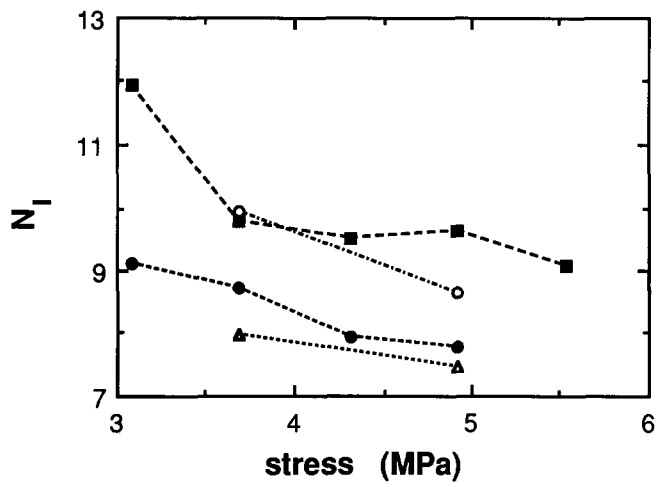

Figure 17 Number of crystalline blocks per layer *versus* the applied stress at different temperatures. Same symbols as in *Figure 4*

blocks for important loads or eventually to the merging of some crystal blocks along direction b. The coalescence of the crystalline blocks can unfortunately not be assessed with certainty. Indeed, the kinetics of deformation is related to the applied load, and the deformation path is not the same for all the samples. Therefore, the total deformation is not the only varying parameter. The nucleation and growth processes can be much dependent on the applied load even at a constant temperature.

To sum up, at a constant temperature, an increase of the stress leads mainly to a thickening of the crystalline layers along direction 1 whereas the mean crystallinity inside a layer remains constant owing to larger crystals along direction 2. These two phenomena are favoured by an increase in orientation.

This improvement of the crystalline order as the temperature is raised can be explained by the following arguments. The size of the crystals increases with temperature and the number of crystals per unit volume decreases slightly with temperature. This means that larger crystals are formed at elevated temperatures because of thermal effects and coalescence of some crystalline blocks. Since all these events occur inside the layers, their crystallinity is increased.

The crystallinity inside a layer is poorly rescaled by

the equilibrium deformation. The layer's crystalline density is essentially a function of temperature as shown above. This observation is in agreement with the fact that the length of the crystallites along direction a increases with temperature. Since this direction tends to be parallel to the OX_3 axis, an increase of the crystal size along this direction acts in favour of an increase of the crystallinity inside a layer.

It is now possible to present a more detailed picture of the respective influences of temperature and stress on the crystalline organization inside the material. At a given temperature (above 85°C in order to establish a well organized structure), the increase of the stress yields a thickening of the crystalline layers along the directions OX_1 and OX_2. As the temperature is raised, the crystalline blocks are larger, leading to an increase in the crystallinity inside a layer.

As far as samples 'stretched with flow' or stretched at the *NDR* are concerned, the SAXS patterns reveal a much less organized structure although layers of crystalline blocks are already present. Therefore, the calculations carried out above become meaningless and lead to unrealistic conclusions.

CONCLUSIONS

In this study, we have reported an experimental characterization of the crystalline phase of PET films, free to deform above T_g under a given stress with a uniaxial-planar symmetry. The structure has been studied for samples having reached an equilibrium deformation under the applied load.

The chain axes exhibit a high level of orientation towards the machine direction, which increases with temperature and stress. The phenyl rings also orient with their plane normals parallel to the thickness direction of the film. Their orientation is also increased as the tension and the temperature are raised.

As samples stretched under crystallizing conditions (i.e. where the strain-induced crystallization is the dominant phenomenon in the deformation) are considered, it has been found that the equilibrium draw ratio is a correlation parameter for the crystallinity, the orientation of the a and c axes. The size of the crystallites along the directions a, b and c can also be rescaled by λ_p although the rates of crystallization along the three directions are different, leading to more subtle effects. For these samples, the crystalline structure appears organized in crystalline blocks gathered into layers inclined at a given angle with respect to the stretching direction. As the temperature is raised, these crystalline layers thicken in the direction of the OX_1 axis (essentially in the temperature range 90–95°C) and their crystallinity increases because of an increase of the crystal's dimensions along the a and b axes. The applied stress has a strong influence at the lowest temperatures as far as the thickness of the crystalline layers is concerned. Otherwise, the amount of the crystalline phase inside a layer is essentially determined by the temperature and not by the stress.

REFERENCES

1 Agassant, J. F., Avenas, P. and Sergent, J. P. La mise en forme des matières plastiques, Tech. & Doc., 1986
2 Le Bourvellec, G., Beautemps, J. and Jarry, J. P. *J. Appl. Polym. Sci.* 1990, **39**, 319
3 Le Bourvellec, G. and Beautemps, J. *J. Appl. Polym. Sci.* 1990, **39**, 329
4 Dulmage, W. J. and Geddes, A. L. *J. Polym. Sci.* 1958, **31**, 499
5 Heffelfinger, C. J. and Burton, R. L. *J. Polym. Sci.* 1960, **47**, 289
6 Heffelfinger, C. J. and Schmidt, P. G. *J. Appl. Polym. Sci.* 1965, **9**, 2661
7 Dumbleton, J. H. and Bowles, B. B. *J. Polym. Sci. (A-2)* 1966, **4**, 951
8 Nobbs, J. H., Bower, D. I. and Ward, I. M. *Polymer* 1976, **17**, 25
9 Casey, M. *Polymer* 1977, **18**, 1219
10 Quian, R., Shen, J. and Zhu, L. *Makromol. Chem., Rapid Commun.* 1981, **2**, 499
11 Matsuo, M., Tamada, M., Terada, T., Sawatari, C. and Niwa, M. *Macromolecules* 1982, **15**, 988
12 Cakmak, M., Spruiell, J. E. and White, J. L. *Polym. Eng. Sci.* 1984, **24**, 1390
13 Jungnickel, B. J. *Angew. Makromol. Chem.* 1984, **125**, 121
14 Cakmak, M., Spruiell, J. E., White, J. L. and Lin, J. S. *Polym. Eng. Sci.* 1987, **27**, 893
15 Heffelfinger, C. J. and Lippert, E. L. *J. Appl. Polym. Sci.* 1971, **15**, 2699
16 Bezruk, L. I., Kawai, T. and Lipatov, Y. S. *Polym. J.* 1974, **6**, 376
17 Fischer, E. W. and Fakirov, S. *J. Mater. Sci.* 1976, **11**, 1041
18 Elsner, G., Zachmann, H. G. and Milch, J. R. *Makromol. Chem.* 1981, **182**, 657
19 Röber, S., Bösecke, P. and Zachmann, H. G. *Makromol. Chem., Macromol. Symp.* 1988, **15**, 295
20 de Vries, A. J., Bonnebat, C. and Beautemps, J. *J. Polym. Sci., Polym. Symp.* 1977, **58**, 109
21 de Daubeny, R., Bunn, C. W. and Brown, C. J. *Proc. R. Soc. Lond. (A)* 1954, **226**, 531
22 Alexander, L. E. 'X-Ray Diffraction Methods in Polymer Science', Wiley, New York, 1969
23 Jungnickel, B. J., Teichgraber, M. and Ruscher, C. *Faserforschung Textiltechnik* 1976, **24**, 423